Title	A damage mechanics approach to modeling failure in Greywacke rock
Author(s)	Pogacnik, Justin; McNamara, David D.; O'Sullivan, Mike; O'Sullivan, John
Publication Date	2014
Publication Information	Pogacnik, Justin, McNamara, David D., O'Sullivan, Mike , & O'Sullivan, John (2014). A Damage Mechanics Approach to Modeling Failure in Greywacke Rock Paper presented at the 36th New Zealand Geothermal Workshop, Auckland.
Publisher	New Zealand Geothermal Workshop
Link to publisher's version	https://www.geothermal-energy.org/publications_and_services/conference_paper_database.html
Item record	http://hdl.handle.net/10379/6709

A DAMAGE MECHANICS APPROACH TO MODELING FAILURE IN GREYWACKE ROCK

Justin Pogacnik[1], David McNamara[2], Mike O'Sullivan[1] and John O'Sullivan[1]

[1]Department of Engineering Science, University of Auckland, 70 Symonds St. Auckland 1142, New Zealand

[2] Department of Geothermal Sciences, GNS Science,

j.pogacnik@auckland.ac.nz

Keywords: *Finite Element Method, greywacke rock, failure, damage mechanics.*

ABSTRACT

Fracture networks within greywacke basement rocks often control fluid flow in geothermal reservoirs in New Zealand. Thermal, hydrological, chemical, and mechanical processes affect the evolution of these fracture networks. Damage mechanics offers a framework that can be used in the numerical modeling of failure and permeability evolution of geothermal rocks. However, no damage mechanics model has been utilized to describe the complex mechanical behavior of greywacke basement rock. In this work, we apply a damage mechanics THM simulation technique to model stress-strain data for greywacke rock from laboratory uniaxial compression and confined compression tests. Calibration of solid mechanics properties for greywacke rock in THM modeling is a necessary step in the simulation of damage and permeability evolution for heat transport in enhanced geothermal systems.

1. INTRODUCTION AND BACKGROUND

Greywacke rocks are widespread throughout New Zealand (Read, Perrin, and Richards (1999)). Much of the nation's infrastructure (e.g., dams, roads) is built in or on greywacke terrain. The rocks are a typical source of road sealing chip and concrete aggregate. Intact, unweathered samples can have an upper compressive strength of about 350 MPa (Read, Perrin, Richards (1999)). Read, Richards, and Perrin (2000) state that greywacke rocks are typically highly fractured with close spacing between defects (> 750 mm between defects is rare). Greywacke basement rock in New Zealand also hosts the producing geothermal reservoirs of a number of geothermal fields in the Taupo Volcanic Zone (TVZ). Within these reservoirs fluid flow in controlled by faulting and fracturing. The success of Engineered Geothermal Systems (EGS) relies on creating a heat exchanger in hot deep basement rock similar to greywacke and that fluid flow is structurally controlled. Therefore, in an engineering simulation regarding deformation in greywacke rocks, it is important to accurately parameterize the model for rock behavior and failure.

There has been a rich history involving the mechanical testing and characterization of greywacke rocks in New Zealand, most of which has been performed by GNS Science (see Read/Richards/Perrin (1999, 2000, 2001, 2007) and McNamara, *et al.* (2014)). Failure strength, elastic modulus, Poisson's ratio, and other material parameters are highly dependent upon the quality of the rock sample, including the degree of fracturing and jointing present. Therefore, it has been difficult for researchers to adequately characterize a typical rock failure criterion (the Hoek-Brown criterion) for greywacke rocks. McNamara, *et al.* (2014) sought to characterize greywacke samples from two different sites, the Waipapa and Torlesse Terranes, in a

variety of mechanical tests – Unconfined Compressive Strength (UCS), triaxial compression, and Brazilian compression tests. They aim of the research discussed here is to calibrate a numerical model to match the data presented in that work.

Failure in geomaterials is generally attributed to the propagation and coalescence of microcracks (Mazars and Pijauder-Cabot (1989)). Damage mechanics is a branch of continuum mechanics that seeks to incorporate microstructural changes at the continuum level by incorporating the influence of microscale history into the solid constitutive equations (De Borst, *et al.* (2012)). Damage mechanics has been applied with success to characterize the stress-strain behavior of geomaterials (*e.g.*, Zhou, *et al.* (2006) and Zhang, *et al.* (2013)). Damage mechanics has also been applied to simulations of hydrofracking and hydroshearing (*e.g.*, Lu, *et al.* (2013) and Pogacnik, *et al.* (2014)).

In this work, we seek to extend our previous damage mechanics work by calibrating a rock damage initiation criterion introduced by Mazars and Pijauder-Cabot (1989) to greywacke rock. As a first step, we calibrated the model for unconfined uniaxial compression experiments. But we seek to simulate a range of experiments including triaxial compression, Brazilian compression, and shear tests to ensure the robustness of the damage algorithm and the initiation criterion. After a brief outline of the balance equations and constitutive relations with damage considerations, we present our numerical experiments and compare the results to laboratory data obtained by GNS.

1.1 Geological Context

Mechanical data from greywacke was obtained using representative samples from greywacke basement terranes known to underlie TVZ geothermal fields, the Waipapa and Torlesse Terranes. Samples of Torlesse Terrane greywacke were sampled from Blue Rock Quarry near Whakatane. The greywacke here has an average grain size of ~0.14 mm, high quartz grain content, and is highly compacted. Greywacke samples of the Waipapa Terrane were sampled from the Waotu Quarry near Tokaroa. Like the Torlesse greywacke samples the rock is very compacted by has a larger average grain size of ~0.25 mm, higher lithic grain content, and lower quartz grain content.

Quarry outcrops from which both greywacke types were sampled display a high level of brittle deformation. Exposed quarry surfaces showed multiple fracture and fault planes with greywacke fragments and grains within slip planes. Older generations of fracture are also present as mineralized (calcite and quartz/silica) veins which display thin alteration halos. Samples selected for laboratory experiments were checked to make sure they had no visible alterations, and contained no structures visible to the naked

eye, thus ensuring the mechanical properties determined were for intact, fresh, undeformed greywacke.

2. BALANCE EQUATIONS

2.1 Linear Momentum Balance for the Rock Matrix

In this work, inertial forces in the solid rock matrix were ignored. The linear momentum balance from Bonet and Wood (2008) is written as:

$$\text{div}\boldsymbol{\sigma} + \mathbf{f} = \mathbf{0} \qquad (1)$$

where the vector $\text{div}\boldsymbol{\sigma}$ is the spatial divergence of the Cauchy stress tensor (to be formally defined in the next section) and $\mathbf{f}$ a vector of body forces (both external and density related). Note that boldface fonts are used to express matrix and vector quantities. The Cauchy stress can be split into two components to represent the effect of pore fluid pressure on the solid matrix (Lewis and Schrefler (1998); Ingebritsen, Sanford, and Neuzil (2006)):

$$\boldsymbol{\sigma} = \boldsymbol{\sigma}'' - \alpha p \mathbf{I} \qquad (2)$$

where $\boldsymbol{\sigma}''$ is Biot's effective stress tensor, α is a constant between 0 and 1, p is the pore fluid pressure, and $\mathbf{I}$ is the identity tensor. The effective stress is defined in terms of strain by Hookes' law:

$$\boldsymbol{\sigma}'' = \mathbf{C}^D : \left(\boldsymbol{\varepsilon} - \boldsymbol{\varepsilon}_T \right) \qquad (3)$$

where $\mathbf{C}^D$ is the fourth order material constitutive tensor and is a function of the damage state, $\boldsymbol{\varepsilon}$ is the strain tensor, ":" represents the double contraction of two tensors, and $\boldsymbol{\varepsilon}_T$ is the thermal strain tensor given by

$$\boldsymbol{\varepsilon}_T = \left(\frac{\beta_S}{3} \right) (\Delta T) \mathbf{I} \qquad (4)$$

Here β_S is the volumetric coefficient of thermal expansion of the solid and ΔT is the change in temperature from the reference state.

2.2 Mass Balance

The pore fluid is assumed to be single phase and consist of fully saturated pure water in this work. The fluid balance equation can be written (from Lewis and Schrefler (1998)):

$$0 = -\left((1-n)\beta_s + n\beta_w \right) \frac{\partial T}{\partial t}$$
$$+ \left(\frac{1-n}{K_s} + \frac{n}{K_w} \right) \frac{\partial p}{\partial t} \qquad (5)$$
$$+ \nabla \cdot \mathbf{v}^s + \nabla \cdot \left\{ \frac{\boldsymbol{\kappa}}{\mu_w} \left[-\nabla p + \rho_w \mathbf{g} \right] \right\} - Q_p$$

where the subscripts s and w refer to the solid and fluid components respectively, t is time, n is the porosity, K are the bulk moduli, $\mathbf{v}_s$ is the velocity of the solid components, $\boldsymbol{\kappa}$ is the permeability tensor, μ_w is the fluid viscosity, ρ_w is the fluid density, $\mathbf{g}$ is the gravity acceleration vector, and Q_p represents fluid mass flow into the system. The derivation of (5) assumes linear dependence of porosity, rock density, and fluid density on pressure and temperature.

2.3 Energy Balance

Lastly, to couple thermal effects, we introduce the energy balance equation, also from Lewis and Schrefler (1998):

$$0 = \left(\rho_w C_w + C_s \rho_s \right) \frac{\partial T}{\partial t}$$
$$+ \rho_w C_w \frac{\boldsymbol{\kappa}}{\mu_w} \left(-\nabla p + \rho_w \mathbf{g} \right) \cdot \nabla T \qquad (6)$$
$$- \nabla \cdot \left\{ \boldsymbol{\chi} \cdot \nabla T \right\}$$

where C represents the specific heat, T is the temperature, ρ_s is the density of the solid, and $\boldsymbol{\chi}$ is the effective thermal diffusivity of the saturated medium. In (6), fluid viscosity and density were taken to be dependent on temperature only. We know that parameters such as permeability and Cauchy stress depend upon the deformation state of the material. One possible theoretical framework for capturing this dependency is damage mechanics. The necessary details for this work will be discussed in the next section.

2. CONSTITUTIVE EQUATIONS

Damage is the process of the initiation and growth of microcracks and cavities (Voyiadjis and Kattan (2005)). At the micro-scale, these phenomena are discontinuous. Damage could be considered as a deterioration process similar to irreversible strain (Besson, *et al.* (2010)). The damage variable is written in terms of stress or strain and can be used in solid mechanics analyses to predict the initiation and evolution of microcracks. These cracks can affect a variety of parameters including, but not limited to, material stiffness and permeability. The damage formulation in this work follows the work presented by Pogacnik, *et al.* (2014), which utilized the yield/damage criterion formulated by Mazars and Pijauder-Cabot (1989).

The first step in damage mechanics is to define the damage variable. We define damage here as a second-order tensor. This allows for either isotropic or anisotropic damage descriptions and is relatively easy to implement and computationally inexpensive. The damage tensor is defined by

$$\mathbf{D} = \sum_k d_k(\cdot) \mathbf{n}_k \otimes \mathbf{n}_k \qquad (7)$$

where $d_k(.)$ is a dimensionless scalar function between 0 and 1 proportional to the amount of theoretical microcracking in a representative volume element. If an element is completely intact without damage, $d_k = 0$; in the completely damaged case, $d_k = 1$.

The damage tensor can be folded into the strain energy density expression for the solid material (Halm and Dragon (1996)):

$$\Psi(\boldsymbol{\varepsilon}, \mathbf{D}) = \frac{1}{2} \lambda \text{tr}(\boldsymbol{\varepsilon})^2 + \eta \boldsymbol{\varepsilon} : \boldsymbol{\varepsilon} + G \boldsymbol{\varepsilon} : \mathbf{D} \qquad (8)$$
$$+ A \text{tr}(\boldsymbol{\varepsilon}) \boldsymbol{\varepsilon} : \mathbf{D} + 2B(\boldsymbol{\varepsilon} : \boldsymbol{\varepsilon}) : \mathbf{D}$$

where λ and η are the Lame parameters (related to Young's modulus and Poisson's ratio), tr(.) is the trace of a tensor, A and B are supplementary constants related to moduli degradation due to damage and G is a constant governing residual damage effects. Taking the first derivative of the strain energy density function with respect to strain gives the Cauchy stress.

$$\boldsymbol{\sigma} = \lambda \text{tr}(\boldsymbol{\varepsilon})\mathbf{I} + 2\eta\boldsymbol{\varepsilon} + G\mathbf{D}$$
$$+A\left[\text{tr}(\boldsymbol{\varepsilon}\mathbf{D})\mathbf{I} + \text{tr}(\boldsymbol{\varepsilon})\mathbf{D}\right] + 2B(\boldsymbol{\varepsilon}\mathbf{D} + \mathbf{D}\boldsymbol{\varepsilon}) \tag{9}$$

The derivative of the Cauchy stress equation with respect to strain yields the fourth-order stiffness tensor. In indicial notation, the form of the stiffness tensor is

$$C_{IJKL}^{D} = \lambda\delta_{IJ}\delta_{KL} + \eta\left(\delta_{IK}\delta_{JL} + \delta_{IL}\delta_{JK}\right)$$
$$+A\left(\delta_{IJ}D_{KL} + D_{IJ}\delta_{KL}\right)$$
$$+B\left(\delta_{IK}D_{JL} + \delta_{IL}D_{JK} + D_{IK}\delta_{JL} + D_{IL}\delta_{JK}\right) \tag{10}$$

Following Mazars and Pijauder-Cabot (1989), damage evolution depends upon a scalar strain function:

$$\xi = \sqrt{\sum_{i=1}^{e}\left(\langle\varepsilon_i\rangle\right)^2} \tag{11}$$

Here the $\langle\varepsilon\rangle$ are MacAulay brackets defined as

$$\langle\varepsilon_i\rangle = \frac{|\varepsilon_i| + \varepsilon_i}{2} \tag{12}$$

where ε_i are the principal strains. This function results in a value of $\langle\varepsilon_i\rangle = \varepsilon_i$ when positive (tension) and $\langle\varepsilon_i\rangle = 0$ when negative (compression).

Damage was computed as a piecewise function of the scalar ξ by

$$D^i = \begin{cases} 0 & \text{if} \quad \xi < \xi_c \\ \dfrac{D_{max}}{\xi_{off} - \xi_c}\xi - D_{max}\dfrac{\xi_c}{\xi_{off} - \xi_c} & \text{if} \quad \xi_c \leq \xi \leq \xi_{off} \\ 1 - (1 - D_{max})\dfrac{\xi_{off}}{\xi} & \text{if} \quad \xi > \xi_{off} \end{cases} \tag{13}$$

where D_{max} was the maximum damage value between 0 and 1 allowed in the simulation, is ξ_c the critical strain value that results in damage initiation, and ξ_{off} is the failure value of the critical strain resulting in a damage of D_{max}.

3. NUMERICAL MODELING
3.1 Numerical Methodology

The simulations in this work were performed using our own in-house THM finite element code written in C++. The code utilizes a Sequential Iterative Approach (SIA) as outlined in Pogacnik, Demspey, *et al.* (2014). Pore fluid pressure and temperature were treated as constants in this work as we were concerned only with matching compression data from greywacke rock samples. Therefore, the SIA was used only for the result of updating the damage

variable and its effect on the solid constitutive relations. As such, the SIA was not strictly necessary for this work. However, it is still a useful implementation for this code as we intend to use it on more complex scenarios with changing pore pressures, temperatures, permeabilities, *etc.* for geothermal applications such as cold-water injection and thermal cracking. During a timestep, we continued to update the damage variable and solve for displacements until the L2-norm in the displacements was below 1.0e-10.

3.2 Simulation Set-up

A 2-D rectangular domain 50 mm x 20 mm was used to represent the laboratory unconfined compression test geometry as seen in Figure 1. The mesh was comprised of 100 x 40 elements for a total of 4141 nodes. We used the laboratory-measured rock density = 2654 kg/m^3 and Young's modulus = 71.0e9 Pa. We set Poisson's ratio = 0.18. The effect of gravity was neglected and simulations were performed at constant atmospheric pressure and room temperature. We set the damage parameters D_{max} = 0.99, ξ_c = 9.0e-4, and ξ_{off} = 2.0e-3. In the solid mechanics equations (8)-(10), we set $A = \lambda/2$, $B = \eta/2$, and $G = 0$ following our previous work (Pogacnik, *et al.* (2014)). Displacement was fixed in both the horizontal and vertical directions on the bottom surface and the top surface was fixed from horizontal displacement, while vertical displacement was specified to a rate of 0.002 mm/s downward. The timestep size of the simulation was 1 s and ran for 20 timesteps.
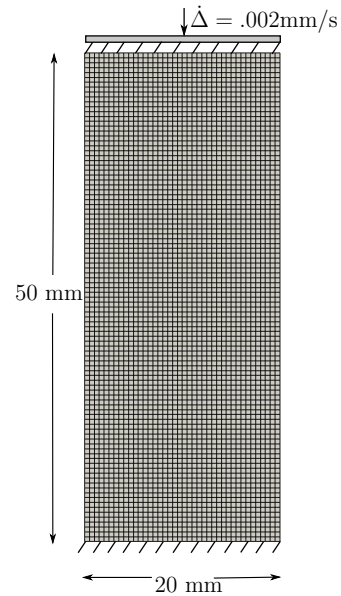

Figure 1. Unconfined Compression Specimen geometry used in finite element simulations in this work.

4. RESULTS AND DISCUSSION

The laboratory test data that we sought to simulate was performed on greywacke rocks with negligible permeability and initial fracture density/porosity. This assumption is based on various laboratory experiment results (McNamara et al., 2014). Very low porosity and permeability measurements combined with a lack of increasing acoustic wave velocity with increasing confining pressures on these greywacke samples imply very little initial open space, or micro-crack presence. Therefore, the specimens were assumed to be as close to a homogeneous material as is possible for rock. Nevertheless, greywacke rocks in the

region do show significant fracturing and there could be a chance that these samples contained small inherent flaws. We therefore simulated both a case with no initial damage distribution and a case with a random initial damage distribution. An initial damage distribution could represent inherent flaws and inclusions within a sample. For this case, we randomly assigned a damage value of 0.1 to 15% of the elements. Practically speaking, this means that the elastic modulus is effectively reduced by 10% in a random 15% of the elements. However, this represents some sort of heterogeneous microcrack structure in the specimen.

Figure 2 displays the results of the engineering stress-strain curve for the laboratory data provided and each finite element simulation. The case with an initial random distribution has a slightly lower Young's modulus and yield stress than the initially undamaged simulation, due to the degradation of the modulus introduced by the damage state. The similarity in the two simulations indicates that small changes in initial state of the specimen do not greatly affect the elastic modulus in uniaxial compression tests, however the initial damage state does make a difference to the failure stress. We chose a value of ξ_{off} that was close to ξ_c, which resulted in brittle behavior during the simulation. That means there was little softening post yield before failure occurred. Where failure is defined as the point where damage has reached D_{max} and propagated a fracture through the entire specimen as seen in Figures 3 and 4 (right).

The residual stiffness seen in the stress-strain response was only due to the definition of $D_{max} = 0.99$. So, even after failure, elements still maintained a small resistance to deformation. This is unphysical behavior, however, specimen failure would have already occurred at this point, so this technique only helps to add numerical stability without sacrificing the ability to simulate failure. Setting $D_{max} = 1.0$ would result in known mesh dependency issues because a fracture singularity cannot be represented in a continuum element without some sort of numerical enrichment.
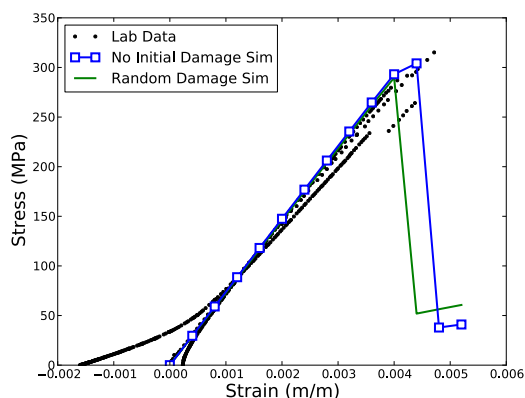

Figure 2. Stress-Strain curve for laboratory data, the initial undamaged uniform simulation, and the initial random damage distribution simulation.

Figures 3 and 4 display the damage results for both the initially undamaged and damaged simulations at three different times. Failure develops along the well-known 45° failure planes associated with brittle materials in each case. The undamaged initial state simulation shows multiple intersecting failure planes that could be indicative of an

explosive failure pattern typically seen in greywacke UCS tests and in compression tests of other rocks. Further, the loading symmetry was obvious in the damage result. However, when a small degree of heterogeneity was added in the initially damaged simulations, a dominant fracture plane emerged in the asymmetric damage distribution. While this was not entirely expected for greywacke rock, the presence of the failure cone-shaped region at the top of Figure 4 (right) is quite common in geomaterial laboratory failure. Even the apparently most uniform rocks have some degree of heterogeneity. Further work is needed to learn how to characterize that heterogeneity with a damage model.
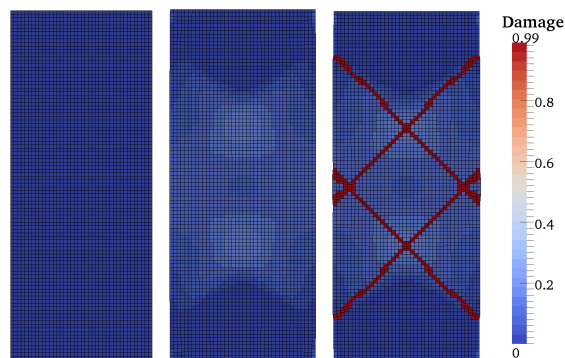

Figure 3. Simulation damage result at t = 0 s (left), 10 s (center), and 12 s (right) for an initially undamaged specimen.
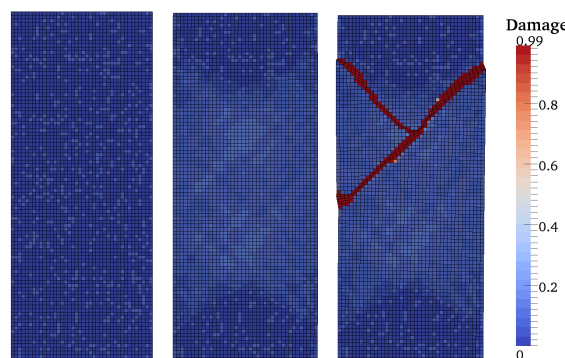

Figure 4. Simulation damage result at t = 0 s, 10 s, and 12 s for a specimen with a random initial damage of 0.1 in 15% of the elements.

5. CONCLUSIONS AND FUTURE WORK

This work is an extension of our previous THM damage mechanics work. It is an initial step forward toward calibrating a damage mechanics model for greywacke basement rock in New Zealand. The continuum damage approach presented in this work, coupled with the Mazars and Pijauder-Cabot initiation criterion is capable of matching laboratory stress-strain data for uniaxial compression tests relatively well. Moving forward, the priority is to apply this model to cold-water injection stimulation simulations and hydrofracking and hydroshearing simulations. However, we first need to investigate the behavior of the model over a range of laboratory tests to ensure the robustness of the failure criterion. We have access to GNS Science's triaxial and

Brazilian compression test data. We are also working to implement this model into the solid mechanics code ABAQUS through use of the User Material Subroutine (UMAT). This would enable us to use this model as a test case for our work involved in coupling AUTOUGH2 with ABAQUS.

ACKNOWLEDGEMENTS

REFERENCES

Besson, J., Cailletaud, G., Chaboche, J., *et al.*: *Nonlinear Mechanics of Materials (Solid Mechanics and Its Applications)*, Springer, (2010).

DeBorst, R., Crisfield, A., *et al.*: *Nonlinear Finite Element Analysis of Solids and Structures*, Ch 6: Damage Mechanics, John Wiley and Sons Ltd, (2012).

Ingebritsen, S., Sanford, W., and Neuzil, C.: *Groundwater in Geologic Processes.* Cambridge University Press, New York. (2006).

Lewis, R., and Schrefler, B.: *The Finite Element Method in the Static and Dynamic Deformation and Consolidation of Porous Media*, John Wiley and Sons, (1998).

Lu, Y., Elsworth, D., and Wang, L.: Microcrack-based Coupled Damage and Flow Modeling of Fracturing Evolution in Permeable Brittle Rocks, *Computers and Geotechnics*, **49**, (2013), 226-244.

Mazars, J. and Pijaudier-Cabot, G.: Continuum Damage Theory – Application to Concrete, *ASCE Journal of Engineering Mechanics*, **115**, (1989), 345-365.

McNamara, D., Faulkner, D. and McCarney, E.: Rock Properties of Greywacke Basement Hosting Geothermal Reservoirs, New Zealand: Preliminary Results. *Proceedings* Stanford Geothermal Workshop (2012).

Pogacnik, J., O'Sullivan, M., and O'Sullivan, J.: A Damage Mechanics Approach to Modeling Permeability Enhancement in Thermo-Hydro-Mechanical Simulations. *Proceedings* Stanford Geothermal Workshop, (2014).

Pogacnik, J., Dempsey, D., Kelkar, S., Podgorney, R., O'Sullivan, M., and O'Sullivan, J.: The Effect of Sequential Solution Procedures in the Numerical Modeling of Stimulation in Engineered Geothermal Systems. *Proceedings*, 11th World Congress for Computational Mechanics, Barcelona, Spain. (2014).

Read, S., Perrin, N., and Richards, L.: Applicability of the Hoek-Brown Failure Criterion to New Zealand Greywacke Rocks. *Proceedings* 9th International Society for Rock Mechanics Congress, Paris, France (1999).

Read, S., Richards, L, and Perrin, N.: Assessment of New Zealand Greywacke Rock Masses with the Hoek-Brown Failure Criterion. *Proceedings* International Society of Rock Mechanics International Symposium, Melbourne, Australia (2000).

Richards, L., Read, S., and Perrin, N.: Comparison of the Hoek-Brown Failure Criterion with Laboratory and Field Test Results for Closely-Jointed New Zealand Greywacke Rocks. *Rock Mechanics: A Challenge for Society* pp. 283-288 (2001).

Richards, L., and Read, S.: New Zealand Greywacke Characteristics and Influences on Rock Mass Behaviour. *Proceedings* 11th Congress of the International Society of Rock Mechanics (2007).

Voyiadjis, G. and Kattan, P.: *Damage Mechanics*, CRC Press, Boca Raton, FL, USA, (2005).

Zhang, R., Jiang, Z., Sun, Q., and Zhu, S.: The Relationship Between the Deformation Mechanism and Permeability of Brittle Rock, *Natural Hazards*, **66**, (2013), 1179-1187.

Zhou, J. Shao, J., Xu, W.: Coupled Modeling of Damage Growth and Permeability Variation in Brittle Rocks, *Mechanics Research Communications*, **33**, (2006), 450-459.